separations

MDPI

Article

Increasing the Accuracy and Optimizing the Structure of the Scale Thickness Detection System by Extracting the Optimal Characteristics Using Wavelet Transform

Abdulilah Mohammad Mayet [1], Tzu-Chia Chen [2,3,*], Seyed Mehdi Alizadeh [4], Ali Awadh Al-Qahtani [1], Ramy Mohammed Aiesh Qaisi [5], Hala H. Alhashim [6] and Ehsan Eftekhari-Zadeh [7,*]

1 Electrical Engineering Department, King Khalid University, Abha 61411, Saudi Arabia
2 College of Management and Design, Ming Chi University of Technology, New Taipei City 243303, Taiwan
3 International College, Krirk University, Bangkok, 3 Ram Inthra Rd, Khwaeng Anusawari, Khet Bang Khen, Bangkok 10220, Thailand
4 Petroleum Engineering Department, Australian University, Kuwait City 13015, Kuwait
5 Department Electrical and of Electronic Engineering, College of Engineering, University of Jeddah, Jeddah 21589, Saudi Arabia
6 Department of Physics, College of Science, Imam Abdulrahman Bin Faisal University, Dammam 31441, Saudi Arabia
7 Institute of Optics and Quantum Electronics, Friedrich Schiller University Jena, Max-Wien-Platz 1, 07743 Jena, Germany
* Correspondence: tzuchiachen1688@gmail.com (T.-C.C.); e.eftekharizadeh@uni-jena.de (E.E.-Z.)

check for updates

Citation: Mayet, A.M.; Chen, T.-C.; Alizadeh, S.M.; Al-Qahtani, A.A.; Qaisi, R.M.A.; Alhashim, H.H.; Eftekhari-Zadeh, E. Increasing the Accuracy and Optimizing the Structure of the Scale Thickness Detection System by Extracting the Optimal Characteristics Using Wavelet Transform. *Separations* **2022**, *9*, 288. https://doi.org/10.3390/separations9100288

Academic Editors: Guoyong Wang and Yan Liu

Received: 27 August 2022
Accepted: 29 September 2022
Published: 5 October 2022

Abstract: Loss of energy, decrement of efficiency, and decrement of the effective diameter of the oil pipe are among the consequences of scale inside oil condensate transfer pipes. To prevent these incidents and their consequences and take timely action, it is important to detect the amount of scale. One of the accurate diagnosis methods is the use of non-invasive systems based on gamma-ray attenuation. The detection method proposed in this research consists of a detector that receives the radiation sent by the gamma source with dual energy (radioisotopes ^{241}Am and ^{133}Ba) after passing through the test pipe with inner scale (in different thicknesses). This structure was simulated by Monte Carlo N Particle code. The simulation performed in the test pipe included a three-phase flow consisting of water, gas, and oil in a stratified flow regime in different volume percentages. The signals received by the detector were processed by wavelet transform, which provided sufficient inputs to design the radial basis function (RBF) neural network. The scale thickness value deposited in the pipe can be predicted with an MSE of 0.02. The use of a detector optimizes the structure, and its high accuracy guarantees the usefulness of its use in practical situations.

Keywords: scale layer thickness; three-phase flow; volume fraction independent; RBF neural network; gas-oil-water separation

1. Introduction

In the oil industry, scale formation inside the transmission pipes causes major problems. The formation of scales makes the internal cross-section of the pipe smaller and reduces the fluid flow, and failure to identify this problem causes malfunctions in pumps and related equipment, emergency shutdowns, damage to oil equipment, increased repair costs, and reduced efficiency. Researchers who considered it necessary to have accurate detection systems to detect the amount of scale inside the pipe always used gamma ray attenuation systems as the gold standard in determining the various parameters of multiphase flows [1–8]. In the study [1], an attempt was made to predict the volume percentage and classification of flow regimes. Using a cesium source, two sodium iodide detectors, and the test pipe, the researchers implemented a two-phase flow in three regimes, stratified, annular, and bubbling, and using the information obtained from both detectors as input for the radial basis function (RBF) network were able to reach their goal. Roshni et al. in [2], at the cost of increasing the computational load to the system, were able to increase the accuracy by using three GMDH networks. Finally, they were able to achieve good accuracy in determining the volume percentage and detecting the type of flow regimes in three-phase flows. In 2016, in similar research, a ^{60}Co source and a NaI detector were used for obtaining the kind of flow patterns and volume percentage, which was met with low accuracy and unfavorable results due to the lack of extraction of appropriate characteristics from the received signals [3]. In 2019, authors used Jaya's optimization algorithm for predicting the volume percentage of a three-phase flow in the stratified pattern [4]. Sattari et al. in [5] proposed a structure with a cesium source and two NaI detectors around the tested pipe to be able to perform volume percentages prediction and classification of flow regimes with high accuracy. The use of time characteristics and the correct selection of characteristics, while reducing the computational load, resulted in a high-precision system. Later research [6] used a GMDH neural network for detecting the kind of flow patterns and predicting the volume percentage. High accuracy was achieved in determining volume percentages, but not considering the amount of scale inside the pipe is one of the gaps in this research. Alamoudi et al. [7] tried for detecting the thickness of scale in the oil pipe. They simulated a two-phase flow in disparate regimes. They considered Gamma peak counts of Ba-133 and Cs-137 from the first transmission photon detector and the total number from the second scattered photon detector as inputs to the RBF neural network, and they were able to foretell the scale thickness with the RMSE of less than 0.22. In another study, the researchers simulated a three-phase flow in the annular pattern by considering the thickness of the scale inside the pipe to inquire into different volume percentages. Finally, the photopeaks ^{241}Am and ^{133}Ba recorded in two transmitted detectors were extracted and considered as the input of an RBF neural network. They predicted the amount of intra-pipe scaling with RMSE of less than 0.09 [8]. In recent years, many researchers have turned to using an X-ray source instead of gamma in their structures, the reason for which is to get rid of problems such as the need to use protective clothing by personnel when working with this device (due to the inability to turn it off) can be stated. They differentiated the parameters of multiphase flows using X-ray tubes [9–12]. For example, in [9], the aforementioned alternative source was used. The training of two existing multilayer perceptron (MLP) neural networks in their proposed structure was also done by the temporal features, which are extracted from the signals received by the detector. In the research [10], three-phase flows were perused, and three patterns were simulated in distinct volume percentages. In this research, three RBF neural networks were trained with the frequency characteristics of the received signals, and the result brought relatively good accuracy. In Ref. [11], an X-ray tube was used for designing a control system. Four petroleum products that are mixed two by two with distinct volumes were simulated with the Monte Carlo N Particle code (MCNP) code. The recorded signals were used as inputs of three MLP neural networks for predicting the volume ratio of the three products. Although the introduced method predicted the type and amount of products, the lack of feature extraction techniques prevented high accuracy. To develop the previous research (Ref. [11]), Balubaid et al. [12] used wavelet transform for feature extraction, which resulted in an effective reduction of computational load and increased accurateness. Numerous studies have been conducted to gauge scale thickness and examine various features [13,14] with more detectors or higher errors. In this study, inspired by the existing history of similar studies, an attempt was made to design a high-precision system to acquire the scale value inside the pipe. For this purpose, a three-phase flow pattern consisting of water, gas, and oil in distinct volume percentages was simulated. A different value of scale thickness was considered in each simulation. A dual-energy gamma source (^{241}Am and ^{133}Ba) and a sodium iodide detector were placed on both sides of a test pipe. From the signals received from the detector, the wavelet characteristics were extracted. These extracted characteristics were considered as the inputs of the RBF neural network to obtain the output, which was the scale thickness inside the pipe. The result of this research is the introduction of an effective and accurate method to detect the amount of scale inside the pipe. The contributions made by this study are as follows:

1. Examining the wavelet transform's properties and effectiveness in calculating scale thickness.
2. Using a single detector lowers costs and the structure of the detecting system's complexity.
3. Increasing the precision of scale thickness determination by extracting useful features from received signals.
4. Using the RBF neural network as a fast-learning network to calculate scale thickness.

2. Simulated Detection System

In recent years, researchers have obtained positive results from radiation-based system simulations with the MCNP code [15–19]. In addition, in this study, the MCNP code has been used. A dual-energy gamma source, a steel test pipe, and a sodium iodide detector are the main parts of the proposed structure. The gamma source consists of radioisotopes ^{241}Am and ^{133}Ba, with photon energies of 59 and 356 keV, respectively. In the simulation of the three-phase flow in the stratified regime, as well as the simulation of the sediment scale, a test pipe made of steel is used, which has an internal diameter of 10 cm and a thickness of 0.5 cm. The detector measuring 2.54 cm^2 is placed at a distance of 30 cm from the source with a zero angle to the assumed line of the source to receive the passing signals. The proposed structure of this study has been validated by the experimental structure implemented in Ref. [1]. This structure of a three-phase flow is simulated in a stratified regime consisting of gas, water, and oil in a volume percentage between 10% to 80%. The deposited scale inside the pipe is considered cylindrical and with a thickness of 0, 0.05, 1, 1.5, 2, 2.5, and 3 cm. The said scale is made of BaSO4 and has a density of 4.5 g per cubic centimeter. Water, oil, and gas considered in this simulation also had densities of 1, 0.826, and 0.00125 g per cubic centimeter. In Ref. [1], a two-phase flow was implemented in the annular regime, and the simulation of the same structure was performed by the MCNP code. The recorded counts obtained from the detectors of the simulated structure and the experimental structure were compared. It was observed that there is an acceptable match between the two. Seven scale thickness values × 36 different volumetric percentages = 252 simulations were performed. Figure 1 shows the proposed structure of this study and how this structure reaches the goal of determining the thickness of the scale. The signals received by the detector are shown in Figure 2. In this figure, the x-axis shows the thickness of the scale, the y-axis represents the source energy, and the z-axis represents the amount of intensity absorbed by the detector.

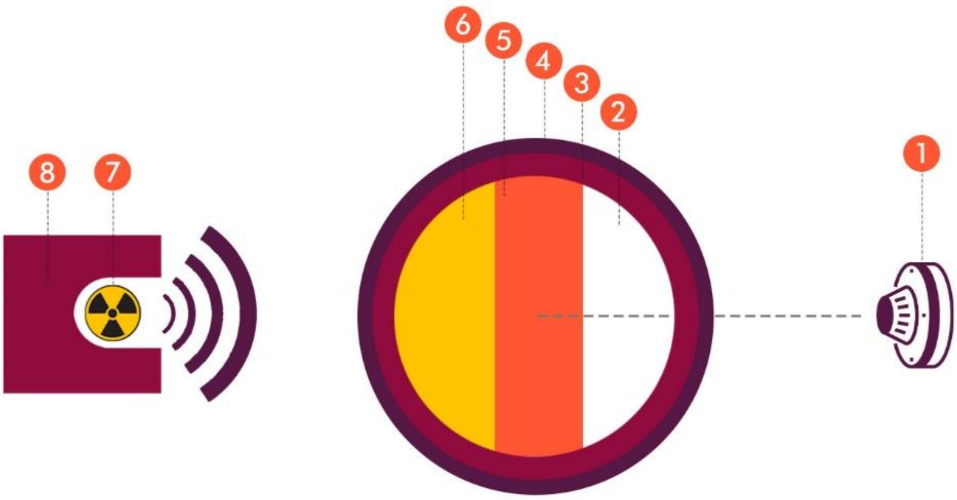

Figure 1. The proposed structure of the detection system: 1-NaI detector, 2-gas phase, 3-scale, 4-steel pipe, 5-water phase, 6-oil phase, 7-dual-energy gamma source, and 8-protective case.

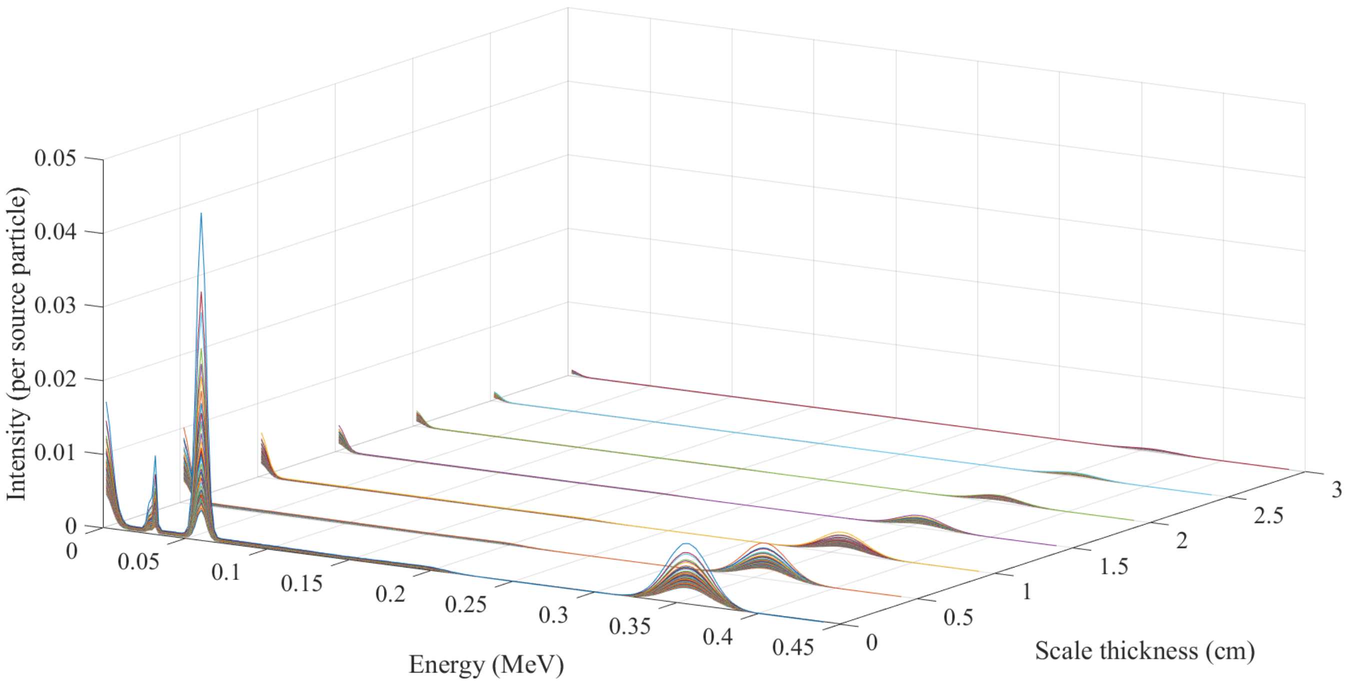

Figure 2. The signal received by the NaI detector.

3. Discrete Wavelet Transform

One of the widely used numerical analyzes is discrete wavelet transform (DWT), in which the wavelet is sampled discretely. In discrete wavelet transform, in addition to frequency features, time features are also available, which is its most important advantage over the Fourier transform. To calculate the DWT of a signal, first, a low-pass filter with the impulse response g is applied to the signal, resulting in the convolution of the two as follows [20,21].

$$y[n] = (x * g)[n] = \sum_{k=-\infty}^{\infty} x[k]g[n-k] \tag{1}$$

In addition, simultaneously, another high pass filter (h) decomposes the signal. Figure 3 clearly shows the signal decomposition process. The output of this process is detail coefficients (output of high-pass filter) and approximate coefficients (output of low-pass filter). At the output of the filters, as seen from the figure, there is a downsampler with 2 in each step. The downsampled results of the low-pass filter provide the approximation (A), and the output of the low-pass samplers of the high-pass filter provides the detail (D). Knowing that at each step, the approximate part can be decomposed over and over again. In this research, the analysis has continued up to four stages. The wavelet operation calculates the wavelet coefficients of a separate set of child wavelets for a given mother wavelet ψ(t). In the case of discrete wavelet transform, the mother wavelet is shifted and scaled by powers of two [20,21].

$$\psi_{j,k} = \frac{1}{\sqrt{2^j}} \psi\left(\frac{t - k2^j}{2^j}\right) \tag{2}$$

where j denotes the scale parameter and k the shift parameter. Since x(t) is a 2N-length signal, the wavelet coefficients derived from it may be thought of as the projection of x(t) onto a wavelet. A member of the above-mentioned discrete wavelet family is a child wavelet if and only if [20,21]:

$$\gamma_{jk} = \int_{-\infty}^{\infty} x(t) \frac{1}{\sqrt{2^j}} \psi\left(\frac{t - k2^j}{2^j}\right) dt \tag{3}$$

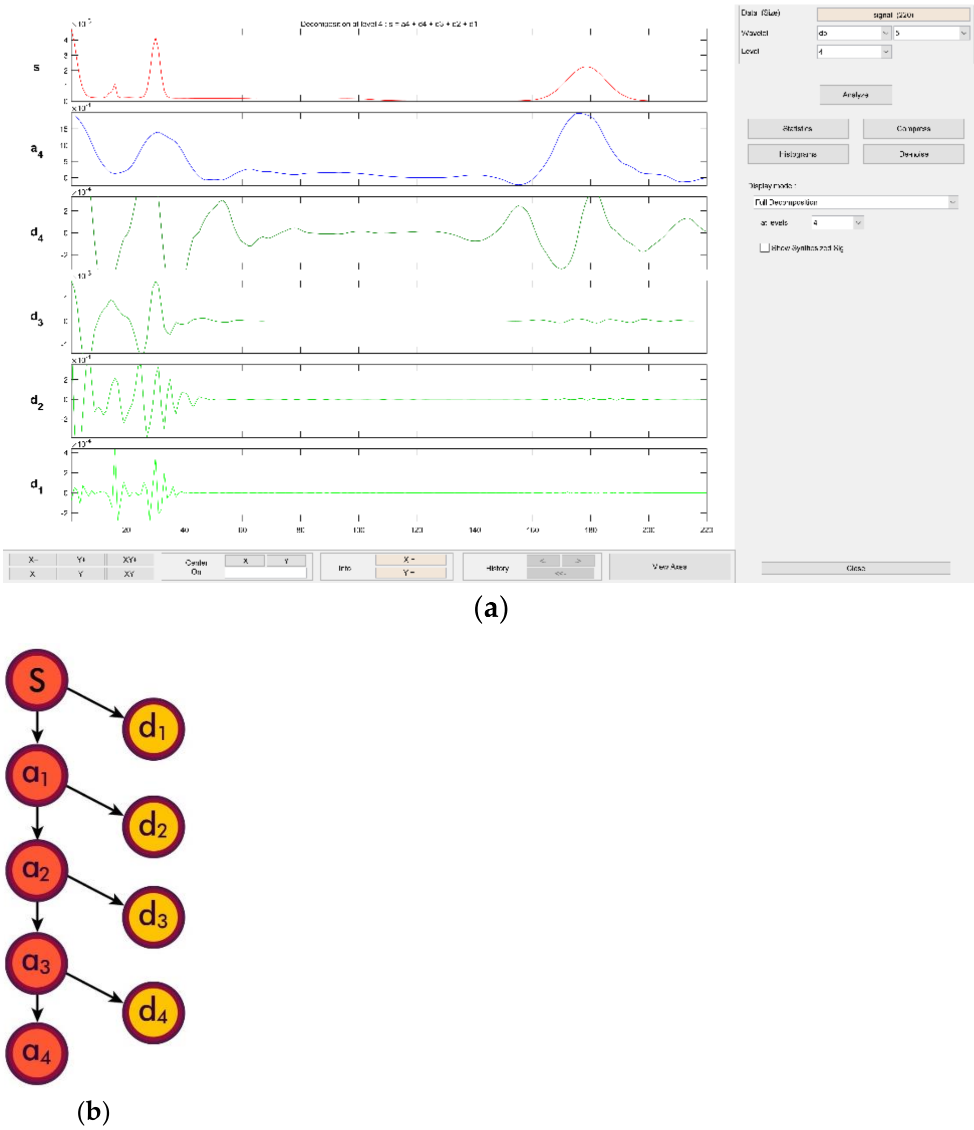

Figure 3. (**a**) Decomposed signal into approximation and details by wavelet transform, (**b**) wavelet transform tree. From each simulation, five characteristics with the names of the mean value of a_4, d_4, d_3, d_2, and d_1 were extracted, in total; a matrix of 5 × 252 was extracted for neural network training.

Then, j is fixed, and the γ_{jk} is obtained only in terms of a function of k. In the above equation, γ_{jk} can be obtained as the convolution of the x(t) with the mother wavelet signal, $h(t) = \frac{1}{\sqrt{2^j}}\psi\left(\frac{-t}{2^j}\right)$, sampled at points 1, 2j. 2j, . . . , 2N. These are details of discrete wavelet coefficients at level j. Detail coefficients of the filter bank, therefore, match perfectly to a wavelet coefficient of a discrete collection of child wavelets for a given mother wavelet ψ(t), assuming an acceptable choice of h[n] and g[n] (t). From the analyzed signals, the characteristics of average of a_4 and average of d_1 to d_4 were extracted and used in the next steps. Since they were originally proposed as useful characteristics in earlier studies [12,22,23], these features have been utilized to improve the accuracy and structure of the scale thickness detection system.

4. RBF Neural Network

Neurons, also known as nerve cells, are the smallest components of the human brain that send and receive signals from the brain. While there are many similarities between neurons and cells, neurons are completely unique in function and structure. All these neurons, which number up to millions, are somehow connected to each other. However, according to their location and responsibility, neurons have three main parts in terms of size, shape, and structure: Cell body, axon, and dendrite. Neurons are actually computing units that have branches called dendrites through which they receive information from other neurons. The neuron's center functions as a processing unit, which then sends the processed data via the axon to neighboring neurons. It all happens biochemically, but researchers have offered ways to describe this architecture mathematically. Radial basis function networks are a popular kind of neural network used to solve this problem (RBF). An RBF network is a kind of convolutional neural network that employs radial basis functions as activation functions. Having been designed for a broad range of purposes, this network has quickly become a popular alternative to the more established multi-layer perceptron. To simplify, RBF employs a three-layer design. There is no processing performed in the input layer since it is a puller layer. Through a non-linear adaptation between the input space and another space with higher dimensions, the second layer (the hidden layer) is able to provide more complex results. The linear output and the final weight total are both generated in the third layer. Such an output is helpful if RBF is used to approximate the function, however, a hard limiter or sigmoid function may be applied to the output neurons to generate 1 or 0 if pattern categorization is necessary. RBF's standout characteristic is the processing that occurs in the hidden layer. This technique's fundamental concept was to generate clusters from preexisting patterns in the input space. The distance from the cluster center may be calculated if its centers are known. Since this is a non-linear distance measure, the result obtained will be close to 1 if a pattern is found in the vicinity of the cluster's center. Outside of this region, the value drops dramatically. The non-linear function may be expressed in terms of the radial basis since this area is radially symmetric around the cluster's center. Radial basis functions often have the following shape [24]:

$$\varphi(r) = \exp\left[-\frac{r^2}{2\sigma^2}\right] \tag{4}$$

The parameter of r in an RBF is the numeral value of the interval from the center of the cluster. Equation (4) shows a typical bell curve. Generally, the measured distance to the cluster center is the Euclidean distance. In the hidden layer, for each neuron, the coordinates of the cluster center are represented by weights. Therefore, when a neuron receives an input pattern X, the interval is obtained using the following equation [24]:

$$r_j = \sqrt{\sum_{i=1}^{n} \left(x_i - w_{ij}\right)^2} \tag{5}$$

This leads to the following output from the j neuron in the hidden layer [24]:

$$\varnothing_j = \exp\,[-\frac{\sum_{i=1}^{n} \left(x_i - w_{ij}\right)^2}{2\sigma^2}] \tag{6}$$

The width or radius of the bell curve is defined by the variable σ and in some cases, it is appointed only experimentally. The hidden layer of an RBF network has units that have weights, and these weights represent the cluster center vector. Weights can be obtained using traditional methods such as the K-Mean algorithm or methods based on the Kohonen algorithm. In any case, the training is done unsupervised, but the expected number of clusters (k) is already selected, then these algorithms obtain the best fit for these clusters. As a strong mathematical tool, numerical computations [25–31] have been used recently for a variety of engineering challenges, most notably, artificial networks [32–44]. The available data are split into two groups: training data and test data, in order to address the issue of over-fitting and under-fitting. The data that the neural network observes and uses to fit the data is included in the training data. Test data are used to evaluate the effectiveness of the neural network following the training phase. The planned network will be protected against the issues of over-fitting and under-fitting by the neural network's suitable reaction to these two sets of data.

5. Result and Discussion

The features introduced in the previous sections were given as inputs to the RBF neural network so that the output, which is a 1 × 252 matrix determines the thickness of the scale inside the pipe. Several neural networks were put into practice, each with a distinct hidden layer of neurons. The structure of the optimal trained network can be seen in Figure 4. This network has five input neurons and one output neuron, which are the extracted characteristics and scale thickness value, respectively. Between the input and output layers, there is a hidden layer with 18 neurons, which is responsible for transferring the input space to the output space. In order to show the proper functioning of the neural network, three fit, regression, and error diagrams were drawn for three categories of all data, training, and testing data in Figure 5. The network output is represented by a blue line in the fitting diagram, whereas the intended output is represented by a black dashed line. In this diagram, the horizontal axis represents the data number, while the vertical axis represents the scale's thickness. Two MSE and RMSE criteria were taken into account while calculating the error value of the implemented network. These criterion equations are as follows:

$$MSE = \frac{\sum_{j=1}^{N} \left(X_j(Exp) - X_j(Pred)\right)^2}{N} \tag{7}$$

$$RMSE = \left[\frac{\sum_{j=1}^{N} \left(X_j(Exp) - X_j(Pred)\right)^2}{N}\right]^{0.5} \tag{8}$$

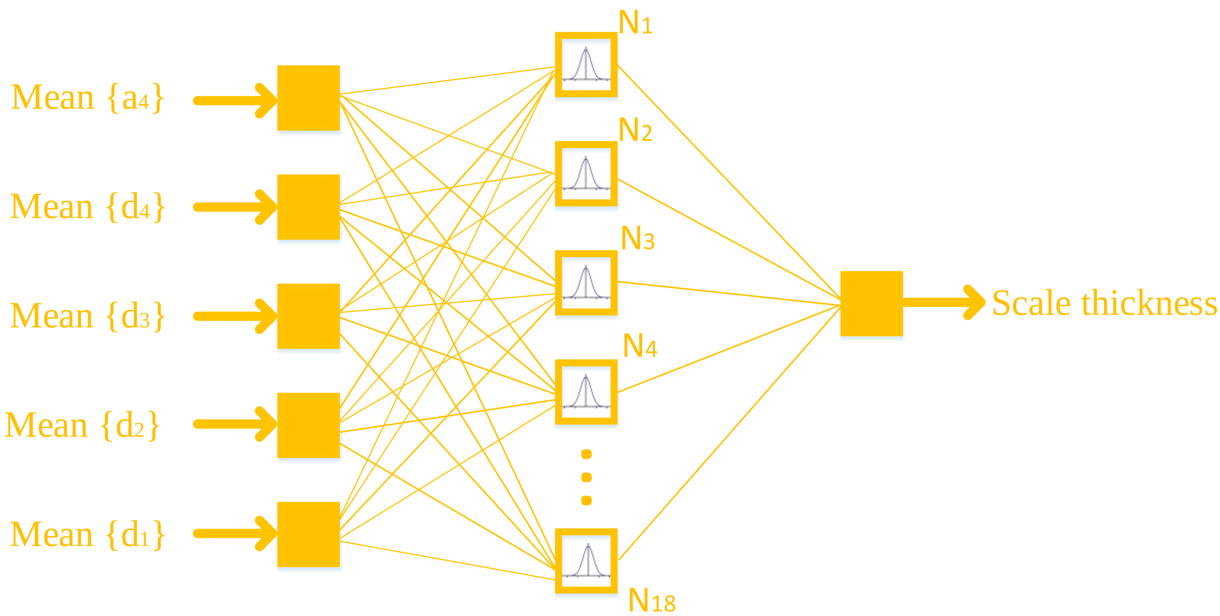

Figure 4. The architecture of the trained RBF neural network.

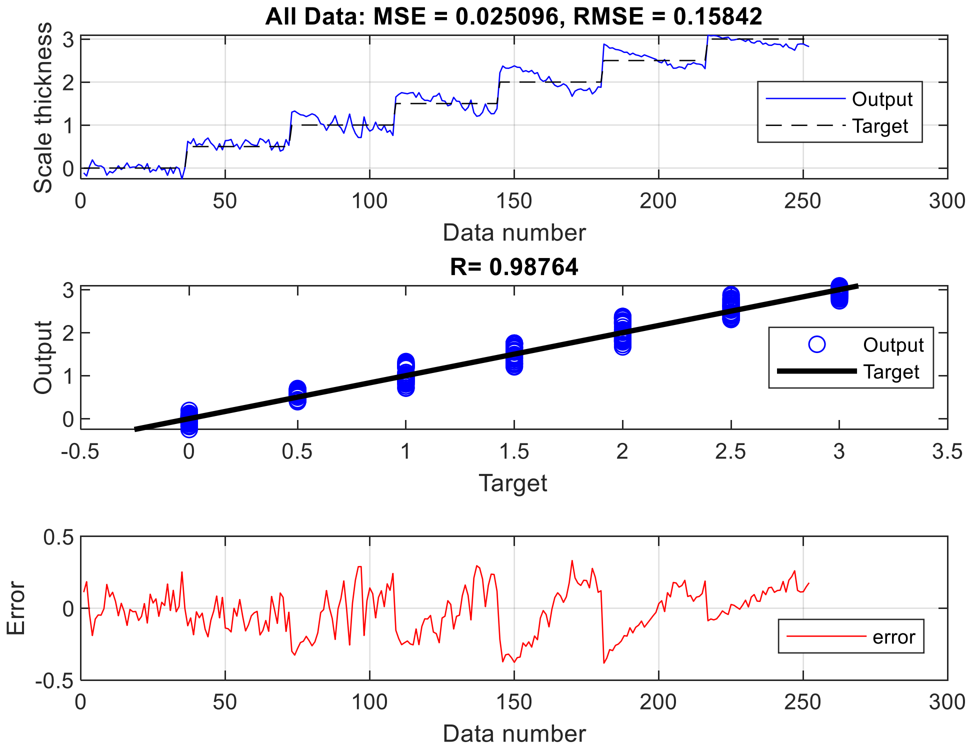

(**a**)

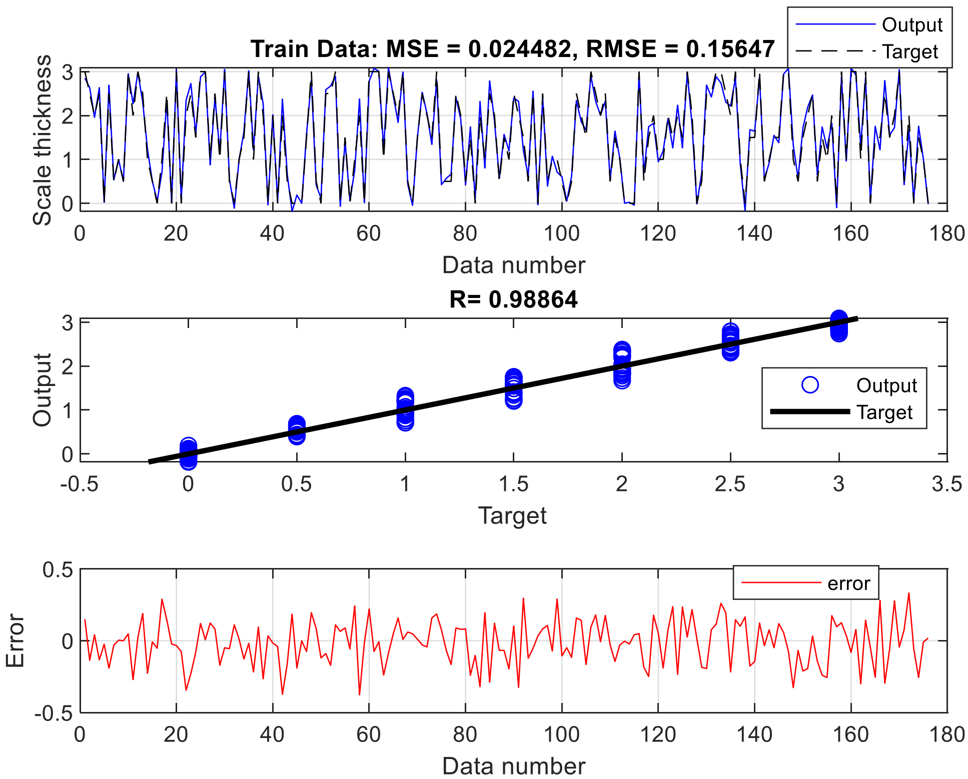

(**b**)

Figure 5. *Cont.*

(**c**)

Figure 5. Neural network performance against (**a**) all data, (**b**) training data, (**c**) and test data.

The symbols "X (Exp)" and "X (Pred)" reflect the experimental and predicted (ANN) values, respectively. N represents the number of data points. The second diagram shows the desired output as a black line and the neural network's outputs as blue squares. Regression diagram is the name given to this illustration. The error figure shows the difference between the network output and the desired output for each data. Table 1 shows the target value of the network and the value predicted by the network. In addition, in Table 2, a comparison is presented in terms of the error rate of the systems introduced in previous research and the detection system in this research. In this research, due to the correct processing of the obtained signals and the training of the neural network with effective characteristics, the error rate has been reported to be significantly low. On the other hand, the effective use of a detector and the reduction of the number of detectors has led to the optimization of the structure and the reduction of the construction cost. According to the present study procedure, the flows through the pipe and the various scale thicknesses inside the pipe were first simulated using the MCNP code, and the signals picked up by the detectors were labeled. Then, five characteristics of the average of a_4 and average of d1 to d_4 were obtained from the signals of each simulation after the received signals had been processed using the wavelet transform. The collected characteristics were used to forecast the scale thickness within the pipe using the RBF neural network. The output of the neural network was compared with the desired output after training to check that it was operating correctly. The main limitation of this study is the need to use protective equipment and clothing when working with radioisotope devices because they have harmful effects on the human body. Using the features and methodology introduced in this research and investigating the performance of different neural networks for productivity in future research are strongly recommended to researchers in this field.

Table 1. Comparison of target values with neural network outputs.

	Train Targets	Train Outputs	Test Targets	Test Outputs
1	3.0000	2.8507	1.5000	1.5502
2	2.5000	2.6358	0	0.0084
3	2.0000	1.9591	1.0000	1.2299
4	2.5000	2.6328	2.5000	2.6055
5	0	0.0246	1.5000	1.4134
6	2.5000	2.6908	2.0000	2.1296
7	0.5000	0.5317	1.0000	0.8584
8	1.0000	0.9959	2.0000	2.2414
9	0.5000	0.5000	2.5000	2.6178
10	3.0000	2.9519	1.5000	1.7279
11	2.0000	2.2706	3.0000	2.8875
12	3.0000	2.9778	0.5000	0.5834
13	2.5000	2.3107	1.0000	0.8300
14	1.0000	1.2258	2.5000	2.5796
15	0.5000	0.5077	3.0000	2.8871
16	0	0.0522	0.5000	0.6381
17	1.0000	0.7109	2.0000	2.2191
18	2.5000	2.3532	0.5000	0.5247
19	0	0.0231	1.5000	1.2896
20	3.0000	3.0335	0.5000	0.6990
21	0	0.0752	1.0000	1.2803
22	2.0000	2.3439	3.0000	2.9794
23	2.5000	2.7286	0.5000	0.5555
24	1.5000	1.5813	2.5000	2.4208
25	3.0000	2.8800	0	0.0852
26	3.0000	2.9935	1.5000	1.5737
27	1.0000	0.8766	2.5000	2.4476
28	2.5000	2.4182	0.5000	0.5218
29	1.0000	1.1707	3.0000	2.8760
30	3.0000	3.0492	1.0000	1.2615
31	0.5000	0.5551	2.5000	2.5231
32	0	−0.1112	0.5000	0.5853
33	1.0000	0.9888	2.0000	1.8922
34	1.5000	1.6268	1.5000	1.4737
35	3.0000	3.0185	1.0000	0.8781
36	1.0000	1.2172	0	−0.1686
37	3.0000	2.9045	2.5000	2.8822
38	2.0000	2.2647	0	−0.0797
39	0	−0.0343	0	−0.2528
40	2.0000	2.0162	2.5000	2.8470
41	0	0.0399	2.5000	2.3918
42	2.0000	2.3730	0	0.0240
43	0.5000	0.6606	1.5000	1.3381
44	0	−0.1847	0.5000	0.6577
45	0	0.1900	2.5000	2.7493
46	0	0.0007	1.5000	1.7535
47	1.5000	1.5749	2.0000	1.8070
48	3.0000	2.8047	2.0000	2.3398
49	0.5000	0.4150	2.0000	2.0685
50	0	0.1194	2.5000	2.7588
51	2.5000	2.5892	1.5000	1.6536
52	2.5000	2.6717	0.5000	0.6614
53	3.0000	2.8893	1.0000	0.8097
54	0	−0.0654	1.5000	1.2968
55	1.5000	1.4104	0	−0.1245
56	0	0.0571	1.0000	0.9329

Table 1. *Cont.*

	Train Targets	Train Outputs	Test Targets	Test Outputs
57	1.0000	0.7580	0	−0.0362
58	2.0000	2.3764	3.0000	2.8228
59	0	0.0156	1.0000	1.0669
60	3.0000	2.7795	2.0000	1.8055
61	3.0000	3.0747	2.5000	2.6317
62	3.0000	3.0070	0.5000	0.5188
63	1.0000	1.2388	1.5000	1.4472
64	3.0000	3.0872	0.5000	0.6452
65	2.5000	2.4517	1.5000	1.5560
66	2.0000	1.8413	2.0000	1.7887
67	3.0000	2.9910	1.0000	1.0048
68	0.5000	0.4394	1.0000	1.2338
69	0	−0.0480	0.5000	0.6543
70	1.5000	1.4888	1.0000	0.8751
71	2.5000	2.5288	0	−0.1118
72	2.0000	2.0434	1.0000	1.0108
73	1.5000	1.3414	2.0000	1.9147
74	3.0000	2.8135	0.5000	0.5529
75	0.5000	0.4246	2.0000	1.8891
76	0.5000	0.5672	2.0000	2.3440
77	0.5000	0.6651		
78	2.5000	2.4111		
79	2.0000	1.9201		
80	0.5000	0.4180		
81	1.5000	1.7401		
82	0	0.1030		
83	2.0000	2.3196		
84	1.0000	0.8052		
85	2.5000	2.7879		
86	2.0000	1.8781		
87	0.5000	0.5666		
88	1.5000	1.5677		
89	1.0000	1.1954		
90	2.5000	2.3980		
91	2.0000	2.3241		
92	1.5000	1.2039		
93	0.5000	0.6220		
94	2.5000	2.5530		
95	0	−0.0323		
96	2.5000	2.4175		
97	0.5000	0.3938		
98	1.0000	1.0718		
99	1.0000	0.7100		
100	0.5000	0.6053		
101	0	0.0484		
102	0.5000	0.6160		
103	2.5000	2.3416		
104	2.0000	1.8580		
105	1.5000	1.6659		
106	3.0000	2.9056		
107	2.5000	2.3207		
108	2.0000	2.0069		
109	2.5000	2.3241		
110	0.5000	0.5279		
111	1.5000	1.6442		
112	1.0000	1.0299		

Table 1. *Cont.*

	Train Targets	Train Outputs	Test Targets	Test Outputs
113	0	0.0031		
114	0	0.0226		
115	0	−0.0417		
116	3.0000	2.9503		
117	0.5000	0.6860		
118	1.5000	1.7487		
119	2.0000	1.8221		
120	1.0000	0.9477		
121	1.0000	1.1897		
122	2.0000	1.9254		
123	1.5000	1.2626		
124	2.0000	2.2340		
125	1.5000	1.2649		
126	3.0000	2.9737		
127	2.0000	1.7831		
128	0	−0.0127		
129	0.5000	0.6844		
130	2.5000	2.6940		
131	2.5000	2.4228		
132	3.0000	2.8849		
133	3.0000	2.7392		
134	2.5000	2.3055		
135	2.0000	2.2171		
136	3.0000	2.8540		
137	1.0000	0.8989		
138	0	−0.1658		
139	1.5000	1.6764		
140	1.5000	1.6445		
141	3.0000	2.8768		
142	0.5000	0.5343		
143	1.0000	0.9241		
144	1.5000	1.5487		
145	1.5000	1.3810		
146	3.0000	2.9438		
147	3.0000	3.0738		
148	1.0000	1.3264		
149	0.5000	0.5668		
150	1.5000	1.7114		
151	2.0000	2.1932		
152	2.5000	2.4678		
153	0.5000	0.6429		
154	1.5000	1.7403		
155	1.0000	1.2559		
156	2.0000	1.8254		
157	0	−0.0976		
158	3.0000	2.8746		
159	1.0000	0.9637		
160	3.0000	3.0812		
161	3.0000	2.9221		
162	1.0000	1.2994		
163	3.0000	2.8575		
164	0	0.0467		
165	1.5000	1.7537		
166	1.5000	1.2195		
167	2.5000	2.7950		
168	1.5000	1.5556		

Table 1. *Cont.*

	Train Targets	Train Outputs	Test Targets	Test Outputs
169	2.0000	1.7226		
170	3.0000	3.0435		
171	0.5000	0.4247		
172	2.0000	1.6679		
173	0	0.0561		
174	1.5000	1.7550		
175	1.0000	1.0100		
176	0	−0.0189		

Table 2. A comparison of the accuracy of the proposed detection system and previous studies.

Ref	Number of Detectors	Extracted Features	Source Type	Type of Neural Network	Maximum MSE	Maximum RMSE
[6]	1	Time features	^{137}Cs	GMDH	1.24	1.11
[5]	2	Time features	^{137}Cs	MLP	0.21	0.46
[45]	1	No feature extraction	^{60}Co	GMDH	7.34	2.71
[46]	2	Frequency features	^{137}Cs	MLP	0.67	0.82
[47]	1	No feature extraction	X-Ray tube	MLP	17.05	4.13
[48]	1	No feature extraction	^{137}Cs	MLP	2.56	1.6
[49]	1	Compton continuum and counts under full energy peaks of 1173 and 1333 keV	^{60}Co	RBF	37.45	6.12
[50]	2	full energy peak (transmission count), photon counts of Compton edge in transmission detector, and total count in the scattering detector	^{137}Cs	MLP	1.08	1.04
[current study]	1	Wavelet features	Dual-energy gamma source	RBF	0.02	0.15

6. Conclusions

Preventing sudden shutdowns and problems in the operation of oil equipment requires detecting the amount of scale inside the oil pipes and dealing with it. In this research, special attention is paid to this need, and an accurate system is used to detect the amount of sediment inside the pipes based on the gamma-ray attenuation technique to measure the thickness parameter of the internal scale of the pipe. The proposed structure for the detection system is simulated using the MCNP code, and a three-phase fluid passage pipe is tested in the stratified regime where scale is present. The dual energy source emits photons on the one hand, and the detector collects them on the other hand of the test pipe. The aforementioned flow was simulated in different volume percentages while different scale values were investigated. Two hundred fifty-two different conditions, including seven scale thickness values from 0 to 3 cm and 36 different volume percentages from 10% to 80%, were simulated. The received signals from the detectors finally led to the extraction of wavelet features, which were the inputs of the RBF neural network. The value of scale thickness was also considered as output in the training phase. The designed neural network had an input layer, a hidden layer, and an output layer, which had 5, 18, and 1 neurons, respectively. The scale thickness in this neural network was predicted by the designed RBF neural network with an MSE of 0.02, which is a much smaller error value according to the results of previous research. Due to its high accuracy, this detection system can be considered a vital part of oil fluid transfer systems, and its use is strongly recommended to oil industry managers. Future research in this area is advised to focus on the application of various neural networks, particularly deep neural networks, in detecting various three-phase current parameters and analyzing the time and frequency characteristics of the received signals.

Author Contributions: Funding acquisition, E.E.-Z.; Investigation, T.-C.C. and S.M.A.; Methodology, A.M.M., A.A.A.-Q., R.M.A.Q. and H.H.A.; Software, A.M.M., A.A.A.-Q., R.M.A.Q. and H.H.A.; Supervision, E.E.-Z.; Writing—original draft, T.-C.C. and S.M.A. All authors have read and agreed to the published version of the manuscript.

Funding: This work was supported by the Deanship of Scientific Research at King Khalid University (Grant numbers RGP.1/243/42). The authors acknowledge support from the German Research Foundation and the Open Access Publication Fund of the Thueringer Universitaets-und Landesbibliothek Jena Projekt-Nr. 433052568; the BMBF-Projekt 05P21SJFA2 Verbundprojekt 05P2021 (ErUM-FSP T05).

Institutional Review Board Statement: Not applicable.

Informed Consent Statement: Not applicable.

Data Availability Statement: Not applicable.

Conflicts of Interest: The authors declare no conflict of interest.

References

1. Nazemi, E.; Roshani, G.H.; Feghhi, S.A.H.; Setayeshi, S.; Zadeh, E.E.; Fatehi, A. Optimization of a method for identifying the flow regime and measuring void fraction in a broad beam gamma-ray attenuation technique. *Int. J. Hydrog. Energy* **2016**, *41*, 7438–7444. [CrossRef]
2. Roshani, M.; Giang, P.; Gholam, H.R.; Robert, H.; Behrooz, N.; Enrico, C.; Ehsan, N. Combination of X-ray tube and GMDH neural network as a nondestructive and potential technique for measuring characteristics of gas-oil–water three phase flows. *Measurement* **2021**, *168*, 108427. [CrossRef]
3. Roshani, G.H.; Nazemi, E.; Feghhi, S.A.H. Investigation of using 60Co source and one detector for determining the flow regime and void fraction in gas–liquid two-phase flows. *Flow Meas. Instrum.* **2016**, *50*, 73–79. [CrossRef]
4. Roshani, G.H.; Karami, A.; Nazemi, E. An intelligent integrated approach of Jaya optimization algorithm and neuro-fuzzy network to model the stratified three-phase flow of gas–oil–water. *Comput. Appl. Math.* **2019**, *38*, 1–26. [CrossRef]
5. Sattari, M.A.; Roshani, G.H.; Hanus, R.; Nazemi, E. Applicability of time-domain feature extraction methods and artificial intelligence in two-phase flow meters based on gamma-ray absorption technique. *Measurement* **2021**, *168*, 108474. [CrossRef]
6. Sattari, M.A.; Roshani, G.H.; Hanus, R. Improving the structure of two-phase flow meter using feature extraction and GMDH neural network. *Radiat. Phys. Chem.* **2020**, *171*, 108725. [CrossRef]
7. Alamoudi, M.; Sattari, M.A.; Balubaid, M.; Eftekhari-Zadeh, E.; Nazemi, E.; Taylan, O.; Kalmoun, E.M. Application of Gamma Attenuation Technique and Artificial Intelligence to Detect Scale Thickness in Pipelines in Which Two-Phase Flows with Different Flow Regimes and Void Fractions Exist. *Symmetry* **2021**, *13*, 1198. [CrossRef]
8. Taylan, O.; Abusurrah, M.; Amiri, S.; Nazemi, E.; Eftekhari-Zadeh, E.; Roshani, G.H. Proposing an Intelligent Dual-Energy Radiation-Based System for Metering Scale Layer Thickness in Oil Pipelines Containing an Annular Regime of Three-Phase Flow. *Mathematics* **2021**, *9*, 2391. [CrossRef]
9. Basahel, A.; Sattari, M.A.; Taylan, O.; Nazemi, E. Application of Feature Extraction and Artificial Intelligence Techniques for Increasing the Accuracy of X-ray Radiation Based Two Phase Flow Meter. *Mathematics* **2021**, *9*, 1227. [CrossRef]
10. Taylan, O.; Sattari, M.A.; Essoussi, I.E.; Nazemi, E. Frequency Domain Feature Extraction Investigation to Increase the Accuracy of an Intelligent Nondestructive System for Volume Fraction and Regime Determination of Gas-Water-Oil Three-Phase Flows. *Mathematics* **2021**, *9*, 2091. [CrossRef]
11. Roshani, G.H.; Ali, P.J.M.; Mohammed, S.; Hanus, R.; Abdulkareem, L.; Alanezi, A.A.; Sattari, M.A.; Amiri, S.; Nazemi, E.; Eftekhari-Zadeh, E.; et al. Simulation Study of Utilizing X-ray Tube in Monitoring Systems of Liquid Petroleum Products. *Processes* **2021**, *9*, 828. [CrossRef]

12. Balubaid, M.; Sattari, M.A.; Taylan, O.; Bakhsh, A.A.; Nazemi, E. Applications of discrete wavelet transform for feature extraction to increase the accuracy of monitoring systems of liquid petroleum products. *Mathematics* **2021**, *9*, 3215. [CrossRef]
13. Mayet, A.M.; Chen, T.-C.; Alizadeh, S.M.; Al-Qahtani, A.A.; Alanazi, A.K.; Ghamry, N.A.; Alhashim, H.H.; Eftekhari-Zadeh, E. Optimizing the gamma ray-based detection system to measure the scale thickness in three-phase flow through oil and petrochemical pipelines in view of stratified regime. *Processes* **2022**, *10*, 1866. [CrossRef]
14. Mayet, A.M.; Chen, T.-C.; Ahmad, I.; Tag Eldin, E.; Al-Qahtani, A.A.; Narozhnyy, I.M.; Guerrero, J.W.G.; Alhashim, H.H. Application of neural network and dual-energy radiation-based detection techniques to measure scale layer thickness in oil pipelines containing a stratified regime of three-phase flow. *Mathematics* **2022**, *10*, 3544. [CrossRef]
15. Pelowitz, D.B. *MCNP-X TM User's Manual, Version 2.5.0*; LA-CP-05e0369; Los Alamos National Laboratory: Los Alamos, NM, USA, 2005.
16. Hosseini, S.; Taylan, O.; Abusurrah, M.; Akilan, T.; Nazemi, E.; Eftekhari-Zadeh, E.; Bano, F.; Roshani, G.H. Application of Wavelet Feature Extraction and Artificial Neural Networks for Improving the Performance of Gas–Liquid Two-Phase Flow Meters Used in Oil and Petrochemical Industries. *Polymers* **2021**, *13*, 3647. [CrossRef]
17. Sattari, M.A.; Korani, N.; Hanus, R.; Roshani, G.H.; Nazemi, E. Improving the performance of gamma radiation based two phase flow meters using optimal time characteristics of the detector output signal extraction. *J. Nucl. Sci. Technol.* **2020**, *41*, 42–54.
18. Iliyasu, A.M.; Mayet, A.M.; Hanus, R.; El-Latif, A.A.A.; Salama, A.S. Abd El-Latif, and Ahmed, S. Salama. Employing GMDH-Type Neural Network and Signal Frequency Feature Extraction Approaches for Detection of Scale Thickness inside Oil Pipelines. *Energies* **2022**, *15*, 4500. [CrossRef]
19. Mayet, A.M.; Salama, A.S.; Alizadeh, S.M.; Nesic, S.; Guerrero, J.W.G.; Eftekhari-Zadeh, E.; Nazemi, E.; Iliyasu, A.M. Applying data mining and artificial intelligence techniques for high precision measuring of the two-phase flow's characteristics independent of the pipe's scale layer. *Electronics* **2022**, *11*, 459. [CrossRef]
20. Daubechies, I. The wavelet transform, time-frequency localization and signal analysis. *IEEE Trans. Inf. Theory* **1990**, *36*, 961–1005. [CrossRef]
21. Soltani, S. On the use of the wavelet decomposition for time series prediction. *Neurocomputing* **2002**, *48*, 267–277. [CrossRef]
22. Eftekhari-Zadeh, E.; Bensalama, A.S.; Roshani, G.H.; Salama, A.S.; Spielmann, C.; Iliyasu, A.M. Enhanced Gamma-Ray Attenuation-Based Detection System Using an Artificial Neural Network. *Photonics* **2022**, *9*, 382. [CrossRef]
23. Mayet, A.M.; Alizadeh, S.M.; Kakarash, Z.A.; Al-Qahtani, A.A.; Alanazi, A.K.; Alhashimi, H.H.; Eftekhari-Zadeh, E.; Nazemi, E. Introducing a Precise System for Determining Volume Percentages Independent of Scale Thickness and Type of Flow Regime. *Mathematics* **2022**, *10*, 1770. [CrossRef]
24. Hartman, E.J.; Keeler, J.D.; Kowalski, J.M. Layered neural networks with Gaussian hidden units as universal approximations. *Neural Comput.* **1990**, *2*, 210–215. [CrossRef]
25. Lalbakhsh, A.; Mohamadpour, G.; Roshani, S.; Ami, M.; Roshani, S.; Sayem, A.S.M.; Alibakhshikenari, M.; Koziel, S. Design of a compact planar transmission line for miniaturized rat-race coupler with harmonics suppression. *IEEE Access* **2021**, *9*, 129207–129217. [CrossRef]
26. Hookari, M.; Roshani, S.; Roshani, S. High-efficiency balanced power amplifier using miniaturized harmonics suppressed coupler. *Int. J. RF Microw. Comput. Aided Eng.* **2020**, *30*, e22252. [CrossRef]
27. Lotfi, S.; Roshani, S.; Roshani, S.; Gilan, M.S. Wilkinson power divider with band-pass filtering response and harmonics suppression using open and short stubs. *Frequenz* **2020**, *74*, 169–176. [CrossRef]
28. Jamshidi, M.; Siahkamari, H.; Roshani, S.; Roshani, S. A compact Gysel power divider design using U-shaped and T-shaped resonators with harmonics suppression. *Electromagnetics* **2019**, *39*, 491–504. [CrossRef]
29. Roshani, S.; Jamshidi, M.B.; Mohebi, F.; Roshani, S. Design and modeling of a compact power divider with squared resonators using artificial intelligence. *Wirel. Pers. Commun.* **2021**, *117*, 2085–2096. [CrossRef]
30. Roshani, S.; Azizian, J.; Roshani, S.; Jamshidi, M.B.; Parandin, F. Design of a miniaturized branch line microstrip coupler with a simple structure using artificial neural network. *Frequenz* **2022**, *76*, 255–263. [CrossRef]
31. Khaleghi, M.; Salimi, J.; Farhangi, V.; Moradi, M.J.; Karakouzian, M. Application of artificial neural network to predict load bearing capacity and stiffness of perforated masonry walls. *CivilEng* **2021**, *2*, 48–67. [CrossRef]
32. Dabiri, H.; Farhangi, V.; Moradi, M.J.; Zadehmohamad, M.; Karakouzian, M. Applications of Decision Tree and Random Forest as Tree-Based Machine Learning Techniques for Analyzing the Ultimate Strain of Spliced and Non-Spliced Reinforcement Bars. *Appl. Sci.* **2022**, *12*, 4851. [CrossRef]
33. Zych, M.; Petryka, L.; Kępiński, J.; Hanus, R.; Bujak, T.; Puskarczyk, E. Radioisotope investigations of compound two-phase flows in an open channel. *Flow Meas. Instrum.* **2014**, *35*, 11–15. [CrossRef]
34. Zych, M.; Hanus, R.; Wilk, B.; Petryka, L.; Świsulski, D. Comparison of noise reduction methods in radiometric correlation measurements of two-phase liquid-gas flows. *Measurement* **2018**, *129*, 288–295. [CrossRef]
35. Golijanek-Jędrzejczyk, A.; Mrowiec, A.; Hanus, R.; Zych, M.; Świsulski, D. Uncertainty of mass flow measurement using centric and eccentric orifice for Reynolds number in the range $10{,}000 \leq Re \leq 20{,}000$. *Measurement* **2020**, *160*, 107851. [CrossRef]
36. Alanazi, A.K.; Alizadeh, S.M.; Nurgalieva, K.S.; Nesic, S.; Grimaldo Guerrero, J.W.; Abo-Dief, H.M.; Eftekhari-Zadeh, E.; Nazemi, E.; Narozhnyy, I.M. Application of Neural Network and Time-Domain Feature Extraction Techniques for Determining Volumetric Percentages and the Type of Two Phase Flow Regimes Independent of Scale Layer Thickness. *Appl. Sci.* **2022**, *12*, 1336. [CrossRef]

37. Mayet, A.M.; Hussain, A.M.; Hussain, M.M. Three-terminal nanoelectromechanical switch based on tungsten nitride—An amorphous metallic material. *Nanotechnology* **2015**, *27*, 035202. [CrossRef]
38. Shukla, N.K.; Mayet, A.M.; Vats, A.; Aggarwal, M.; Raja, R.K.; Verma, R.; Muqeet, M.A. High speed integrated RF–VLC data communication system: Performance constraints and capacity considerations. *Phys. Commun.* **2022**, *50*, 101492. [CrossRef]
39. Mayet, A.; Smith, C.E.; Hussain, M.M. Energy reversible switching from amorphous metal based nanoelectromechanical switch. In Proceedings of the 2013 13th IEEE International Conference on Nanotechnology (IEEE-NANO 2013), Beijing, China, 5–8 August 2013; IEEE: Piscataway, NJ, USA, 2013; pp. 366–369.
40. Khaibullina, K. Technology to remove asphaltene, resin and paraffin deposits in wells using organic solvents. In Proceedings of the SPE Annual Technical Conference and Exhibition, Dubai, United Arab Emirates, 26–28 September 2016; Available online: https://onepetro.org (accessed on 21 September 2022). [CrossRef]
41. Tikhomirova, E.A.; Sagirova, L.R.; Khaibullina, K.S. A review on methods of oil saturation modelling using IRAP RMS. In *IOP Conference Series: Earth and Environmental Science*; IOP Publishing: Bristol, UK, 2019; Volume 378, p. 012075.
42. Khaibullina, K.S.; Korobov, G.Y.; Lekomtsev, A.V. Development of an asphalt-resin-paraffin deposits inhibitor and substantiation of the technological parameters of its injection into the bottom-hole formation zone. *Period. Tche Quim.* **2022**, *17*, 769–781. [CrossRef]
43. Khaibullina, K.S.; Sagirova, L.R.; Sandyga, M.S. Substantiation and selection of an inhibitor for preventing the formation of asphalt-resin-paraffin deposits. *Period. Tche Quim.* **2020**, *17*, 541–551. [CrossRef]
44. Mayet, A.M.; Alizadeh, S.M.; Nurgalieva, K.S.; Hanus, R.; Nazemi, E.; Narozhnyy, I.M. Extraction of Time-Domain Characteristics and Selection of Effective Features Using Correlation Analysis to Increase the Accuracy of Petroleum Fluid Monitoring Systems. *Energies* **2022**, *15*, 1986. [CrossRef]
45. Roshani, M.; Sattari, M.A.; Ali, P.J.M.; Roshani, G.H.; Nazemi, B.; Corniani, E.; Nazemi, E. Application of GMDH neural network technique to improve measuring precision of a simplified photon attenuation based two-phase flowmeter. *Flow Meas. Instrum.* **2020**, *75*, 101804. [CrossRef]
46. Hosseini, S.; Roshani, G.H.; Setayeshi, S. Precise gamma based two-phase flow meter using frequency feature extraction and only one detector. *Flow Meas. Instrum.* **2020**, *72*, 101693. [CrossRef]
47. Roshani, M.; Ali, P.J.M.; Roshani, G.H.; Nazemi, B.; Corniani, E.; Phan, N.H.; Tran, H.O.; Nazemi, E. X-ray tube with artificial neural network model as a promising alternative for radioisotope source in radiation based two phase flowmeters. *Appl. Radiat. Isot.* **2020**, *164*, 109255. [CrossRef] [PubMed]
48. Gholipour Peyvandi, R.; Islami Rad, S.Z. Application of artificial neural networks for the prediction of volume fraction using spectra of gamma rays backscattered by three-phase flows. *Eur. Phys. J. Plus* **2017**, *132*, 1–8. [CrossRef]
49. Roshani Gholam, H.; Ehsan, N.; Farzin, S.; Mohammad, A.I.; Salar, M. Designing a simple radiometric system to predict void fraction percentage independent of flow pattern using radial basis function. *Metrol. Meas. Syst.* **2018**, *25*, 2.
50. Roshani, G.H.; Nazemi, E.; Feghhi, S.A.H.; Setayeshi, S. Flow regime identification and void fraction prediction in two-phase flows based on gamma ray attenuation. *Measurement* **2015**, *62*, 25–32. [CrossRef]